Localization and transport of excitation energy in inhomogeneous supramolecular arrays

Vlaming, Sebastiaan Maarten

Chapter 5

Exchange broadening and non-universal scaling in Lévy disordered chains

We theoretically study Frenkel exciton chains with uncorrelated diagonal disorder obeying Lévy stable distributions with a stability index $\alpha < 1$. These distributions are characterized by heavy tails and divergent second moments. We show that this dramatically alters the optical and localization properties of the Frenkel excitons as compared to those known for Gaussian disorder. In particular, we predict the novel effect of exchange broadening of the absorption spectra and a nonuniversal localization length distribution, caused by the coexistence of two distinct localization mechanisms.[1]

5.1 Introduction

In 1924, Lévy [155] introduced a class of probability distributions that have the unique property of being stable, i.e., if a random variable x is distributed according to the probability density $p(x)$, then any linear combination of independent copies of x, $y = \sum_{n=1}^{N} a_n x_n$, obeys the same type of distribution. This property is well-known for Gaussian distributions (and then is a special case of the central limit theorem), but Lévy generalized the stability concept to a class of distributions

[1] This chapter is based on a manuscript by A. Eisfeld, S. M. Vlaming, V. A. Malyshev, and J. Knoester, submitted.

with a divergent second moment, also known as heavy-tailed distributions, which for large $|x|$ fall off slower than $1/|x|^3$.

A fascinating aspect of Lévy's heavy-tailed distributions is that while they were initially introduced as mathematical curiosities, during the past 20 years it has been recognized that they frequently occur in physics. Examples are anomalous diffusion [157] and noise [158] in complex systems, random walks of polymer segments [159] and chains [160], Lévy flights in trapping of incoherent atomic radiation [161] as well as diffusion of light in materials with strong density fluctuations [162], anomalous stationary states and super-diffusion in non-equilibrium plasmas [163], and non-Lorentzian spectral line shapes of impurities in glasses [164, 165]. Even in biology (optimal searching strategy for randomly placed target sites [166]) and economics [167] Lévy's distributions occur.

In the above examples, Lévy statistics apply to a single random variable x, such as the displacement of a diffusing particle or the mean-free path of light. Collective properties of interacting degrees of freedom which individually obey heavy-tailed Lévy statistics have received little or no attention so far. Several physical situations can be envisioned for which this would be relevant. For example, this situation may arise for degrees of freedom that interact with a collection of randomly distributed multipoles in their surroundings, see Section 4.A. In addition, analogous to the central limit theorem for distributions with a finite second moment, an average over parameters described by heavy-tailed distributions leads to a Lévy distribution. As a result, Lévy disorder might be caused by a large number of interactions which are described by heavy-tailed distributions. Examples of collective excitations where this may happen are electrons in heavily-doped semiconductors [168], magnons in a host with stochastic magnetic impurities, and excitons in molecular aggregates in a glassy host [165].

In this chapter, we will show that the collective properties in such systems may be drastically different from those with more traditionally considered types of disorder, such as Gaussian or box-like distributions. We will do this by investigating Frenkel exciton chains for which the site energies are taken from heavy-tailed Lévy distributions. We will find remarkable collective optical properties that differ even qualitatively from the well-studied case of Gaussian disorder [65]. Examples are exchange broadening of the absorption line shape, the appearance of fine structure in the density of states and the absorption spectrum with increasing disorder strength, and a nonuniversal disorder scaling of the distribution of exciton localization lengths.

5.2 Model

The model we consider describes the example of excitons in molecular aggregates mentioned above. It consists of a linear array of two-level molecules with parallel transition dipoles, which interact through dipole-dipole transfer interactions. The optical excitations of this system are described by the eigenstates of the Frenkel exciton Hamiltonian

$$\hat{H} = \sum_{n=1}^{N} E_n \left|n\right\rangle\left\langle n\right| - J \sum_{n=1}^{N-1} \left(\left|n+1\right\rangle\left\langle n\right| + \left|n\right\rangle\left\langle n+1\right|\right) \ , \tag{5.2.1}$$

where for simplicity only nearest-neighbor couplings are included; the transfer integral $J > 0$ is taken to be constant. Disorder is included by taking the site energies E_n as uncorrelated stochastic variables, drawn from a distribution $p(E)$. Special for our model, as compared to previous studies, is that we consider heavy-tailed Lévy distributions for $p(E)$. In particular, we consider the class of symmetric Lévy distributions with mean zero, given by [156]

$$p(E) = \frac{1}{2\pi} \int_{-\infty}^{\infty} dt e^{iEt} \exp\left(-|\sigma t|^{\alpha}\right) \ . \tag{5.2.2}$$

Here, $\sigma > 0$ and $0 < \alpha \leq 2$ are called the scale parameter and index of stability, respectively. The former determines the half-width at half maximum (HWHM) of $p(E)$ and we will hereafter refer to it as the disorder strength, while the latter fixes the asymptotic behavior $p(E) \sim 1/E^{1+\alpha}$ for $E \gg \sigma$ and $\alpha < 2$. For $\alpha = 2$ and $\alpha = 1$, $p(E)$ reduces to a Gaussian and a Lorentzian (Cauchy) distribution, respectively. It may be checked that indeed these distributions are stable for $0 < \alpha \leq 2$.

It is useful to rewrite the Hamiltonian in terms of the homogeneous exciton solutions $|k\rangle$ of Eq. 5.2.1,

$$\left|n\right\rangle = \left(\frac{2}{N+1}\right)^{1/2} \sum_{k=1}^{N} \sin\frac{\pi k n}{N+1} \left|k\right\rangle . \tag{5.2.3}$$

The above equation is in fact simply the Fourier transform of Eq. 2.1.7. The Hamiltonian can then be separated in a part containing the homogeneous contribution, and a second part that involves the scatterings between the various exciton states,

$$H = \sum_{k=1}^{N} E_k \left|k\right\rangle\left\langle k\right| + \sum_{k,k'=1}^{N} \xi_{kk'} \left|k\right\rangle\left\langle k'\right| , \tag{5.2.4}$$

with the homogeneous exciton energies $E_k = -2J\cos\frac{\pi k}{N+1}$, and the scattering amplitudes

$$\xi_{kk'} = \frac{2}{N+1}\sum_n x_n \sin\frac{\pi kn}{N+1}\sin\frac{\pi k'n}{N+1}. \tag{5.2.5}$$

The second, stochastic part of the Hamiltonian fully accounts for the disorder-induced effects. In particular, the diagonal elements ξ_{kk} correspond to shifts in the transition energy and its probability distribution describes the inhomogeneous broadening of the exciton levels. The disorder-induced scatterings between the homogeneous exciton states $\xi_{kk'}$ leads to localization of the exciton states. Note that while Eq. 5.2.4 holds generally, the above interpretation in terms of deviations from the homogeneous situation is only valid if the scattering term in Eq. 5.2.4 does not dominate, i.e. if the disorder amplitude is not too large.

The probability distribution for the scattering matrix elements in Eq. 5.2.5 can be straightforwardly calculated, which has been done in Section 4.B. Due to the stability of the Lévy distributions, this again yields a Lévy distribution with the same stability index α, but a renormalized width. Likewise, the average site energy for a particular disorder realization on the chain, $\bar{E} = N^{-1}\sum_{n=1}^{N} E_n$, also obeys the same type of distribution, with the same index of stability, but a renormalized disorder strength:

$$\sigma^* = \sigma N^{\frac{1-\alpha}{\alpha}} \ . \tag{5.2.6}$$

For a Gaussian distribution ($\alpha = 2$) this reduces to the well-known result $\sigma^* = \sigma/\sqrt{N}$, which reflects the exchange narrowing effect of the optical line shape of molecular J aggregates [80]: the energy distribution of delocalized excitons is narrower than σ, because they average over the Gaussian energy fluctuations of the individual sites. By analogy one expects from Eq. (5.2.6) that for $\alpha \leq 1$, this effect does not occur. The Lorentzian case ($\alpha = 1$) is special, as it yields $\sigma^* = \sigma$. This case was studied in Ref. [95] and Chapter 4 of this thesis; while it does not exhibit exchange narrowing, its main properties still are similar to those for Gaussian disorder. Here, we are particularly interested in distributions with $\alpha < 1$, for which $\sigma^* > \sigma$ (exchange broadening). We note, however, that the analytical arguments presented below also hold for $1 \leq \alpha \leq 2$.

5.3 Numerical results

We analyzed our model by numerical simulations. We used the algorithm described in Ref. [169] to generate the random energies E_n, after which the Hamiltonian was diagonalized numerically and the optical and localization properties of the exciton eigenstates were determined [65]. The results presented in Figs. 5.3.1 - 5.4.1 were

obtained for $\alpha = 1/2$, using chains of $N = 200$ sites and averaging over tens of thousands of disorder realizations.

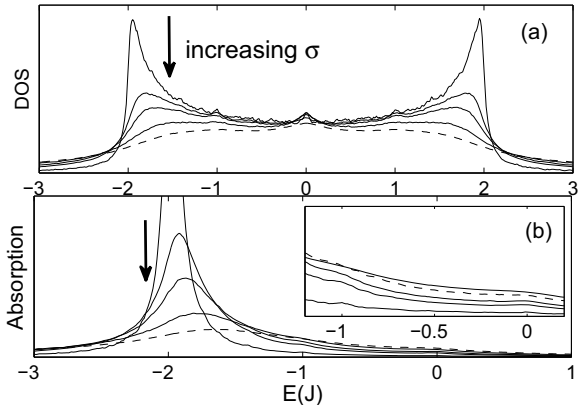

Figure 5.3.1: DOS (a) and absorption spectra (b) for Lévy disorder with $\alpha = 1/2$ and disorder strengths $\sigma = 0.01J$, $0.1J$, $0.2J$, $0.5J$, and J. The arrows mark the curves in order of increasing σ.

Figure 5.3.1 shows the DOS and the absorption spectrum for various disorder strengths σ. The DOS exhibits a typical one-dimensional (1D) shape, with peaks at the band edges $E = \pm 2J$ that are smeared by disorder. However, three additional features are visible: one at the band center, $E = 0$, and two more at $E = \pm J$. The relative importance of these three features strongly depends on σ, revealing a transition from a 1D excitonic DOS to a mostly monomeric DOS with increasing σ. The origin of the extra features, which we found to get more pronounced upon decreasing α, will be explained below.

The additional structure in the DOS is also reflected in the absorption spectrum [Fig. 5.3.1(b)]. While this spectrum is dominated by the intense band edge peak, characteristic for J aggregates, two much less intense features occur at $E = -J$ and $E = 0$. For Gaussian or Lorentzian disorder these features cannot be discerned. Figure 5.3.1(b) also reveals another new effect, with increasing value of σ, the J band shifts to the blue, while for Gaussian disorder a red-shift occurs [65].

Figure 5.3.2 displays the HWHM of the absorption band as a function of σ, for $\alpha = 1/2$ (crosses) and for comparison also for $\alpha = 2$ (Gaussian; circles). This plot confirms the most fascinating effect of heavy-tailed Lévy distributions, anticipated above, namely the occurrence of exchange broadening: While for Gaussian disorder the HWHM is smaller than the bare disorder σ, for $\alpha = 1/2$ it is

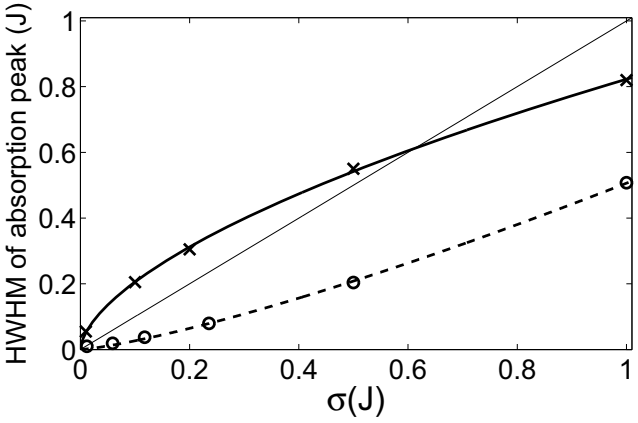

Figure 5.3.2: The HWHM of the absorption spectrum as a function of σ for Lévy disorder with $\alpha = 1/2$ (crosses) and for Gaussian disorder (circles). The corresponding power law fits are plotted as a solid and a dashed line, respectively. The thin solid line HWHM $= \sigma$ is plotted for reference.

larger (for $0 < \sigma < 0.6$). The best power-law fit to the data for $\alpha = 1/2$ reads HWHM $= 0.85J\,(\sigma/J)^{0.6}$ (solid line), which differs markedly from the well-known scaling HWHM $\propto J\,(\sigma/J)^{4/3}$ for the Gaussian case (dashed line) [65]. While the broadening effect qualitatively agrees with Eq. (5.2.6), we will see below that the quantitative explanation of the scaling exponent 0.6 is more subtle.

Finally, Fig. 5.3.3 characterizes the distribution $P(N_{\rm loc})$ of the localization length of the exciton states that occur in the energy interval $[-2.1J, -1.9J]$, i.e., around the lower band edge $E_b = -2J$, the region that dominates the optical response and low-temperature exciton transport. Shown are the numerical data (symbols) and their power-law fits (lines) for the average, $\bar{N}_{loc}$, (crosses and solid line) and the standard deviation, δN_{loc}, (dots and dashed line) of $P(N_{\rm loc})$ as a function of σ. The power-law fits represent the data very well, and read $\bar{N}_{loc} = 2.56(J/\sigma)^{0.36\pm0.01}$ and $\delta N_{\rm loc} = 0.91(J/\sigma)^{0.43\pm0.02}$. The scaling exponents will be discussed in more detail Section 5.4. Thus, the ratio $\delta N_{loc}/\bar{N}_{loc}$ is not constant, implying that, in contrast to Gaussian and Lorentzian disorder (see Chapter 4), Lévy disorder with $\alpha < 1$ does not lead to a universal function for $P(N_{\rm loc})$ in the σ-range considered. This can be clearly observed from the inset of Fig. 5.3.3, where $P(N_{\rm loc})$ is plotted for $\sigma = 0.001J$ and $\sigma = 0.1J$, after scaling the horizontal

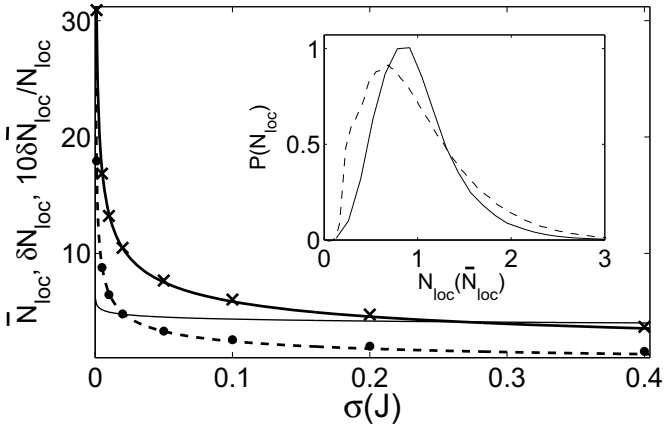

Figure 5.3.3: The average, $\bar{N}_{\rm loc}$, (crosses) and the standard deviation, $\delta N_{\rm loc}$, (dots) of the localization length distribution $P(N_{\rm loc})$ as functions of σ for Lévy disorder with $\alpha = 1/2$. The thick solid and dashed lines are power-law fits, respectively (see text). The thin solid line gives $10(\delta N_{\rm loc}/\bar{N}_{loc})$, while the inset shows the localization length distributions for $\sigma = 0.001J$ (dashed) and for $\sigma = 0.1J$ (solid).

axis to the average localization length appropriate for the σ value considered. We note that the scaling relations described here, only weakly depend on the choice of the energy interval around E_b.

5.4 Discussion

The explanation of all phenomena found above, lies in the interplay between two mechanisms for localizing the exciton states around E_b by heavy-tailed Lévy disorder. For Gaussian disorder only one such mechanism exists, namely the fact that random site energies create local effective potential wells in which the states localize. It has been shown that the typical localization length N^* of these states can be obtained from comparing their level separation to their mixing rate [66] (see also Section 4.2.3). Generalizing these arguments to the case of Lévy distributions yields

$$N^* = \left(\frac{3\pi^2 J}{\xi_\alpha \sigma} \right)^{\frac{\alpha}{1+\alpha}}, \tag{5.4.1}$$

where ξ_α is a numerical factor of order unity ($\xi_{1/2} \approx 0.7$). For $\alpha = 1/2$, this gives $N^* \propto (J/\sigma)^{1/3}$. We note that the scaling exponent $1/3$ is very close to the one obtained above for $\bar{N}_{\rm loc}$ (which was 0.36 ± 0.01), confirming the applicability of the simple scaling arguments discussed in Ref. [66] and Section 4.2.3. However, the second moment is observed to scale with a different exponent; this implies that the shape of the localization length distribution is not universal, but varies for different values of the disorder strength. Combining Eq. 5.4.1 with the renormalized disorder strength Eq. 5.2.6 allows us to express the exciton HWHM in terms of the HWHM of the monomer distribution,

$$\sigma_\xi / J \propto (\sigma/J)^{\frac{2\alpha}{1+\alpha}} . \tag{5.4.2}$$

For Gaussian disorder, N^* is the only length scale relevant to the band edge states and the optical response. In the case of the heavy-tailed Lévy distributions, however, a second localization mechanism - and corresponding length scale - exists. The long tails lead to a high concentration of outliers, i.e., sites with energy $|E_n| > 2J$. These fluctuations are so large that the interaction J cannot overcome them; they therefore break up the chain in segments of length $N_{\rm seg}$, capped by two outliers, which form the maximum intervals over which excitons may delocalize. A similar situation occurs in the case of Lorentzian disorder ($\alpha = 1$), as in Section 4.3, however, for decreasing α values this effect gets stronger. Indeed, in the case of Lorentzian disorder, outliers will also occur, but are too infrequent to have a noticeable effect on the localization length distribution. It is straightforward to show that for $\alpha \leq 1$ the segment length distribution is exponential (see Section 5.A), with mean

$$\bar{N}_{\rm seg} = \frac{\pi}{2\Gamma(\alpha)\sin(\pi\alpha/2)} \left(\frac{2J}{\sigma}\right)^\alpha . \tag{5.4.3}$$

$\bar{N}_{\rm seg}$ is the second length scale in the problem.

The existence of two different localization mechanisms is nicely confirmed by Fig. 5.4.1, which for $\alpha = 1/2$ and $\sigma = 0.1J$ shows a typical realization of the exciton wave functions and energies in the neighborhood of the lower exciton band edge and well below it. We first note that, indeed, we observe quite a few outliers, with positions indicated by the vertical dashed lines. Each outlier has a strongly localized s-like exciton state outside of the band associated with it (lower panel); not all these states are seen, as several of them have energies outside the range of the plot. With regards to the two localization mechanisms, three situations may be distinguished, each of which occurs in Fig. 5.4.1.

(i) $N^* < N_{\rm seg}$. This is the situation common for Gaussian disorder. Near the lower band edge one then typically finds doublets of s- and p-type states, roughly

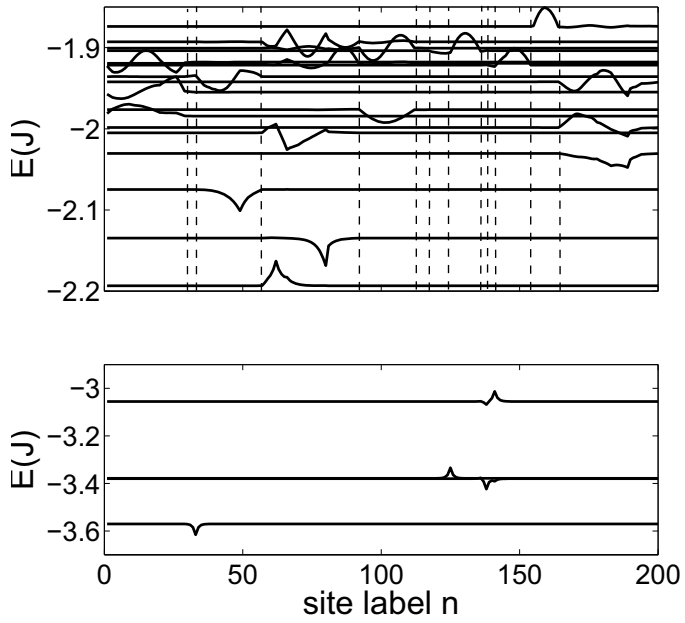

Figure 5.4.1: Exciton wave functions and energies for a typical realization of Lévy disorder with $\sigma = 0.1J$ and $\alpha = 1/2$. The upper panel focuses on energies around the lower band edge; the lower panel displays an energy interval deep in the DOS tail. The dashed vertical lines indicate the positions of outliers in the site energy.

localized on the same interval [66]. In Fig. 5.4.1 this occurs between $N = 52$ and $N = 96$.

(ii) $N^* \approx N_{\rm seg}$. Here one finds multiplets of three or more states on a single segment, which resemble the states of a disorder-free chain of size $N_{\rm seg}$. In Fig. 5.4.1 examples occur between $n = 1$ and $n = 31$, between $n = 92$ and $n = 112$, and between $n = 164$ and $n = 200$,

(iii) $N^* > N_{\rm seg}$. In this case the segmentation strongly confines the excitons and the states within a segment typically get further separated than in the absence of segmentation. If the segments are still relatively large, their lowest s-like eigenstates contain considerable oscillator strength and occur just above the band edge (e.g., the state between $n = 154$ and $n = 164$ in Fig. 5.4.1). With increasing value

of σ, the segments get shorter and the energy of the s-like state increases. This explains the blue-shift of the J band observed in Fig. 5.3.1(b). Also, for growing σ, segments of length 1 and 2 become more likely. These give rise to states with energies distributed around the average monomer and dimer energies, $E = 0$ and $E = \pm J$, respectively, thus explaining the extra features in the DOS and the absorption spectra observed in Fig. 5.3.1. Closer scrutiny even reveals features for segments of length 3, 4, etc, but these are weak and overshadowed by the band edge peaks. For smaller values of α, these features become more prominent. To illustrate this, Fig. 5.4.2 shows the density of states and the absorption spectrum for a Lévy disordered chain with $\alpha = 1/4$ and $\sigma = 0.1J$. Not only the monomer and dimer peaks at $E = 0$ and $E = \pm J$, but also trimer peaks at $E = 0, \pm\sqrt{2}J$ and higher order peaks can clearly be observed.

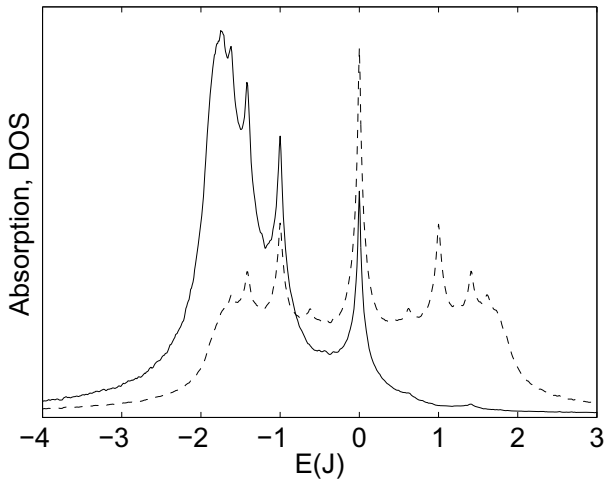

Figure 5.4.2: The density of states (dashed line) and the absorption spectrum (solid line) for a Lévy disordered chain with $\sigma = 0.2J$ and $\alpha = 1/4$.

Of course, the existence of two localization mechanisms, each with its own length scale, is directly responsible for the observed nonuniversality of the localization length distribution. Moreover, the interplay between both mechanisms also explains the disorder scaling of the exchange broadening of the absorption band. Using Eq. (5.2.6) and replacing N by either N^* or $\bar{N}_{\rm seg}$, we obtain the contributions to the HWHM from the states localized by the two different mechanisms, respec-

tively. This leads to HWHM$^* \propto J(\sigma/J)^{2\alpha/(1+\alpha)}$ and HWHM$_{\rm seg} \propto J(\sigma/J)^{1-\alpha}$. For $\alpha = 1/2$, the scaling exponent equals $2/3$ and $1/2$, respectively. Since the numerically obtained exponent equals 0.60 ± 0.03, we conclude that both scales, N^* and $\bar{N}_{\rm seg}$, almost equally contribute to the disorder scaling of the J band width.

5.5 Summary

In summary, we have shown that heavy-tailed Lévy disorder has dramatic consequences for the properties of systems with collective excitations. Novel effects occur, such as exchange broadening and a nonuniversal scaling of the distribution of exciton localization lengths. We have shown that these effects may all be traced back to the simultaneous occurrence of two different localization mechanisms, each with its own length scale, namely the conventional localization caused by small local variations in energy and the segmentation-related localization caused by outliers. We have used the Frenkel exciton chain as an example, but we expect that the occurrence of two localization length scales has equally dramatic effects on other disordered systems with collective excitations, such as those mentioned in the introduction.

Appendix 5.A Occurrence of segment boundaries

Lévy distributions are characterized by heavy tails, implying that there is a relatively high probability for sites to acquire energies lying outside of the exciton band ($-2J \leq E \leq 2J$ for a homogeneous system); we will refer to such a site as an outlier.

The probability for a site to be an outlier is evaluated as

$$P_{\rm b} = 1 - \int_{-2J}^{2J} dx\, p(x) = 1 - \frac{1}{\pi} \int_{-\infty}^{\infty} dt\, \frac{\sin 2Jt}{t}\, \exp\left(-|\sigma t|^{\alpha}\right) \ . \tag{5.A.1}$$

If we restrict ourselves to moderate disorder strengths $\sigma \ll J$, the expression in Eq. (5.A.1) can be evaluated explicitly. In that case, we have $2J \gg \sigma$, and only the range $|2Jt| < 1$ will contribute significantly to the integral. Using a Taylor expansion of the exponential, $\exp\left(-|\sigma t|^{\alpha}\right) = 1 - |\sigma t|^{\alpha}$, one obtains

$$P_{\rm b} = \frac{2}{\pi} \left(\frac{\sigma}{2J}\right)^{\alpha} \int_0^{\infty} dt\, t^{\alpha-1} \sin t = \frac{2}{\pi} \Gamma(\alpha) \sin\left(\frac{\pi\alpha}{2}\right) \left(\frac{\sigma}{2J}\right)^{\alpha} \ , \tag{5.A.2}$$

where $\Gamma(\alpha)$ is the Euler Gamma function. The mean number of barriers in a chain

of N sites is thus $\bar{N}_{\rm b} = NP_{\rm b}$, allowing us to estimate the mean segment size as

$$\bar{N}_{\rm seg} = \frac{N}{N_{\rm b}} = \frac{\pi}{2\Gamma(\alpha)\sin(\pi\alpha/2)} \left(\frac{2J}{\sigma}\right)^{\alpha}. \tag{5.A.3}$$

Since a segment consists of two boundaries separated by $N_{\rm seg}$ sites, the distribution of segment lengths is exponential,

$$P(N_{\rm seg}) = P_{\rm b}^2 \left(1 - P_{\rm b}\right)^{N_{\rm seg}}. \tag{5.A.4}$$